

# RGBD-Glue: General Feature Combination for Robust RGB-D Point Cloud Registration

Congjia Chen<sup>1</sup>, Xiaoyu Jia<sup>2</sup>, Yanhong Zheng<sup>2</sup>, and Yufu Qu<sup>1</sup>

<sup>1</sup> Beihang University

<sup>2</sup> Beijing Institute of Spacecraft System Engineering

**Abstract.** Point cloud registration is a fundamental task for estimating rigid transformations between point clouds. Previous studies have used geometric information for extracting features, matching and estimating transformation. Recently, owing to the advancement of RGB-D sensors, researchers have attempted to utilize visual information to improve registration performance. However, these studies focused on extracting distinctive features by deep feature fusion, which cannot effectively solve the negative effects of each feature’s weakness, and cannot sufficiently leverage the valid information. In this paper, we propose a new feature combination framework, which applies a looser but more effective fusion and can achieve better performance. An explicit filter based on transformation consistency is designed for the combination framework, which can overcome each feature’s weakness. And an adaptive threshold determined by the error distribution is proposed to extract more valid information from the two types of features. Owing to the distinctive design, our proposed framework can estimate more accurate correspondences and is applicable to both hand-crafted and learning-based feature descriptors. Experiments on ScanNet show that our method achieves a state-of-the-art performance and the rotation accuracy of 99.1%.

**Keywords:** Point cloud registration · Feature combination · Correspondences estimation

## 1 Introduction

Point cloud registration, which aligns partial views of a scene, is a key component in numerous tasks, such as SLAM and robotics applications. Researchers typically use methods that rely on correspondence extraction and geometric fitting to estimate the geometric transformation between two point clouds. Here, correspondence extraction is crucial, as high-quality correspondences can effectively reduce computation and improve the accuracy of geometric fitting.

Correspondence extraction can be categorized into two components: feature extraction and correspondence estimation. For feature extraction, a representative hand-crafted feature descriptor is FPFH [41], and recent learning-based feature descriptors [1, 3, 12, 29] have been improved significantly by learning more distinctive features. However, even with the learning-based feature descriptors,

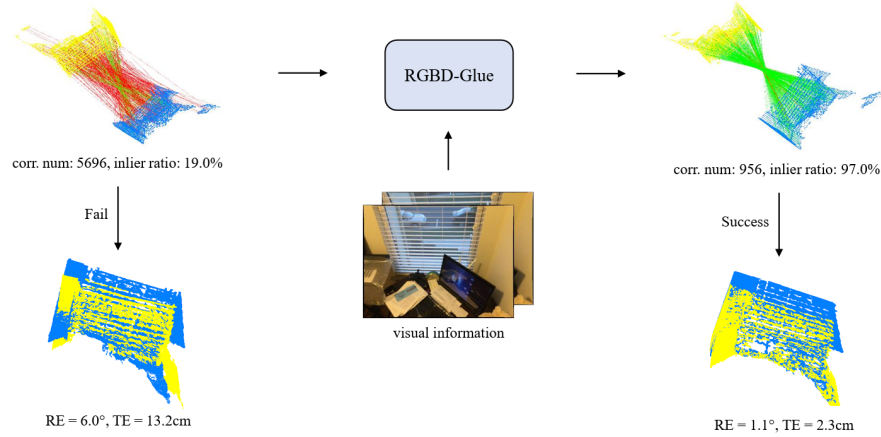


**Fig. 1:** RGBD-Glue combines visual and geometric features to estimate credible correspondences for geometric fitting, which can achieve low rotation errors (REs) and translation errors (TEs) in registration.

the low inlier ratio is still a hard problem to any correspondence-based geometric fitting methods. To this end, correspondence estimation methods are used to find more inliers. Recent studies have used CNN [11], PointNet [24] or attention module [37, 56] to improve the inlier ratio, and have achieved remarkable performance. Although these methods are effective, they incur additional training costs, and their generalization performance is not always promising.

The aforementioned methods are based only on geometric information. Owing to the rapid popularization of inexpensive RGB-D cameras, the acquisition of RGB-D data has become easier, thus facilitating the use of visual information. In recent studies [18, 19, 51, 57], visual information has been used for point cloud registration, which demonstrated a state-of-the-art performance. However, UR&R [18] uses only point clouds for localization and does not fully leverage geometric information. Meanwhile, BYOC [19] uses visual correspondences as labels to bootstrap feature learning, which does not sufficiently exploit the correlation between visual and geometric features. LLT [51] and PointMBF [57] extract fused visual-geometric features to deeply combine the two modalities, but this tight strategy will allow the weakness of one feature to affect another, and cannot sufficiently leverage the valid information of visual and geometric features. Besides, they all focus on training a feature extraction model using both two modalities, which have limited their generalization and flexibility.

In this paper, we aim to propose a method that can combine the two modalities in a more effective and flexible way, and construct a general framework that can be learning-free when needed. Visual feature descriptors can generate more distinctive keypoints and features than geometric feature descriptors, and can achieve a higher accuracy in feature matching [19]. For this reason, visual correspondences can easily achieve a roughly accurate transformation estimation.

However, sparse matches limit their performance and robustness, and make it hard to achieve fine registration. By contrast, geometric feature descriptors are more stable to generate dense and correct correspondences, but heavy outliers pose a considerable challenge to geometric fitting. Inspired by these, we propose a general feature combination framework RGBD-Glue, our key insight is to utilize the complementary properties of visual and geometric features, combine the advantages of the two features to overcome each feature’s weakness.

As mentioned before, it’s easier to estimate a roughly accurate geometric transformation via visual correspondences, which can be served as an useful prior information. Using the transformation, we estimate the error distribution of the assumed inliers and design an adaptive threshold for distribution test. Then, an explicit filter is proposed to extract the geometric correspondences with high transformation consistency and obtain a credible correspondence set. Finally, accurate registration can be achieved via the set. Compared with previous RGB-D fusion studies [18, 19, 51, 57], our proposed method can effectively combine the advantages of visual and geometric features, and avoids performance degradation when one of the two features is weak. Besides, our method focuses on flexibility and makes feature fusion in a looser but more effective way, which brings our method unique advantages and outstanding performance. As shown in Fig. 1, the correct correspondences are obtained and an accurate registration is achieved.

Owing to the design on feature combination, our proposed framework is compatible with any visual and geometric feature descriptors, and can effectively combine visual and geometric features to achieve better performances compared with using individual feature. Benefit from this, our proposed framework is general that it can use diverse feature descriptors for various tasks rather than depending on particular networks. By using hand-crafted feature descriptors, our method does not require learning but is comparable to learning-based methods. Moreover, by using learning-based feature descriptors, our method outperforms other learning-based methods.

For evaluation, we conduct experiments on a large RGB-D indoor dataset ScanNet [14] and compare the performance of our method with those of recent point cloud registration methods. Besides, we conduct comprehensive ablation studies to demonstrate the effects of each component in our method.

In summary, the contributions of this study are as follows:

- We propose a flexible framework that combines visual and geometric features in a simple and novel way to achieve better point cloud registration. The experiments show that our method achieves a state-of-the-art performance.
- We propose a loose feature combination strategy and design an explicit filter based on transformation consistency for reliable correspondence estimation.

## 2 Related Work

### 2.1 Image Feature Matching

Image feature matching uses local features that are sparse keypoints associated with a descriptor to obtain the correspondences between two images.

Classical methods, which rely on hand-crafted keypoint detectors and feature descriptors [5, 31, 35, 39, 40], have been proven to be effective. Meanwhile, learning-based methods used in recent studies [16, 17, 38, 55] have demonstrated outstanding performances. Learning-based methods use CNN to extract more distinctive features, thus significantly improving the accuracy of feature matching.

Local features are typically matched with a nearest-neighbor search in the feature space. In this process, non-matchable keypoints and imperfect features usually result in mismatches. To solve this issue, Lowe’s ratio test [35] is commonly performed to filter the correspondences, and RANSAC [21] is used to identify the optimal model with the maximum number of inliers. In addition, methods based on graph-matching [10, 20, 61] have been proven to be effective, and the excellent performance of learning-based methods has been demonstrated in recent studies [34, 43, 60]. Specifically, learning-based matching methods solve this task as a classification problem, where deep networks are trained to match features and reject outliers [7, 15, 47, 49]. When sufficiently trained, learning-based methods can tolerate heavy outliers and obtain reliable correspondences. In this study, we demonstrate the high accuracy of visual feature correspondences and utilize them to improve the performance of RGB-D point cloud registration.

## 2.2 Point Cloud Registration

Classical methods are ICP-based [6, 44, 45]. They consider the nearest neighbor points as correspondences and estimate the geometric transformation iteratively using an optimization algorithm. In recent studies, most methods have focused on feature extraction [3, 12, 29, 41] and correspondence estimation [9, 37, 56, 59], where transformation is solved using a robust algorithm [21, 53].

FPFH [41] is one of the best hand-crafted descriptors for feature extraction. Recently, several learning-based descriptors [3, 12, 29] with advanced performance have been proposed. However, these descriptors are based only on geometric information. Meanwhile, the popularization of RGB-D cameras renders the utilization of visual information promising. To the best of our knowledge, BYOC [19] demonstrates the manner by which visual correspondences can improve geometric feature learning, and UR&R [18] uses RGB-D data to realize unsupervised learning and achieves an outstanding performance. Subsequently, LLT [51] and PointMBF [57] propose fusion networks to extract fused visual-geometric features and have demonstrated state-of-the-art performance. Our study is inspired by these promising networks. However, instead of feature extraction, we utilize visual and geometric information to achieve better correspondence estimation through an adaptive filter based on transformation consistency.

The main purpose of correspondence estimation is to obtain accurate correspondences for geometric fitting. Early methods ranked correspondences based on feature similarity scores [36] or voting scores [23, 42, 54]. Chen et al. [9] proposed SC2-PCR, which uses a second-order spatial compatibility metric to rank correspondences. Zhang et al. [59] proposed MAC, which uses maximal cliques to obtain consistent sets and generate accurate pose hypotheses. In addition, DGR [11] and PointDSC [2] train networks to remove outliers. CoFiNet [56] and

GeoTransformer [37] apply attention aggregation to extracted features and accurately match correspondences, which have achieved advanced performance in large datasets [22, 58]. Compared with these methods, our method can achieve higher inlier ratio and better registration performance by leveraging both visual and geometric information.

### 2.3 RGB-D Fusion

RGB-D data have two modalities: depth image, which can provide abundant geometric information, and RGB image, which contains valuable visual information. Several methods have been proposed to leverage both modalities. In typical point cloud tasks such as detection [32, 33, 48], segmentation [8, 26–28, 50], and registration [18, 19, 51, 57], the fusion of visual and geometric information improves the performance.

For registration, UR&R [18] directly uses visual information instead of geometric information for feature extraction and matching. BYOC [19] uses visual information to create pseudo-correspondence labels that replace pose supervision and achieve self-supervised registration. LLT [51] uses a local linear transformation module to embed geometric features into visual features and extract fused visual-geometric features. PointMBF [57] combines visual and geometric information with bidirectional fusion, so that visual and geometric feature information can interact with each others, and extracts deep fused features. However, these methods use visual correspondences to create labels for better feature learning, or extract fused visual-geometric feature to deeply combine the two modalities, which cannot effectively combine the advantages of each feature. Differ from these methods, our proposed method uses a looser fusion strategy, which can effectively exploit the complementary information. With an explicit filter consistency and an adaptive threshold calculated by the error distribution, our method is able to effective leverage each feature’s advantages and extract more valid information from the features.

## 3 Method

The framework is illustrated in Fig. 2. We first extract visual and geometric features respectively and match the features to get correspondence sets  $C_{vis}$  and  $C_{geo}$ . Then, we propose an adaptive filter based on transformation consistency to extract valid information and obtain a credible correspondence set  $C$ . Subsequently, we use the set  $C$  to estimate the transformation similarly as in BYOC [19]. Finally, we apply post-refinement to fully leverage the high-quality correspondences estimated using our method. The details of each component are presented in the following sections.

### 3.1 Feature Matching

In our preprocessing step, we split the RGB-D image pair into RGB images  $I_0, I_1 \in \mathbb{R}^{H \times W \times 3}$  and point clouds  $P_0, P_1 \in \mathbb{R}^{N \times 3}$ . Subsequently, we use an

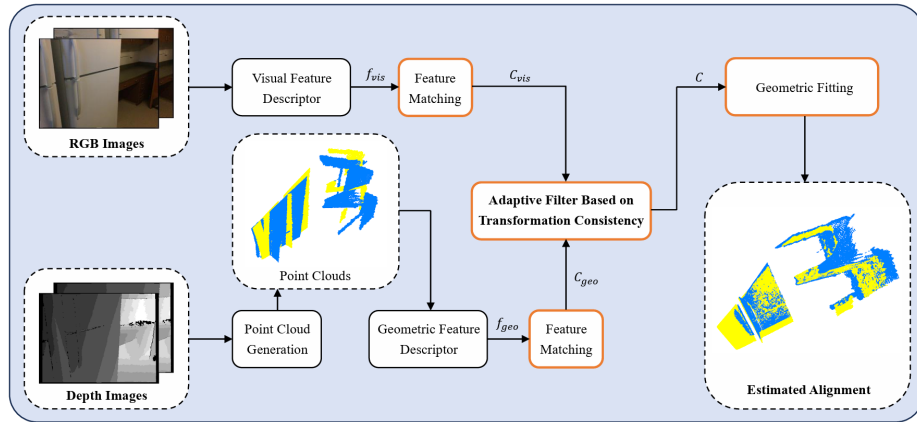


**Fig. 2:** Architecture of the proposed RGBD-Glue framework. First, we extract both visual and geometric features from RGB-D data. Second, we match them to obtain correspondences. Third, we leverage the high-quality visual correspondences to find credible geometric correspondences by testing the transformation consistency based on an adaptive threshold. Finally, we estimate the transformation via the correspondences.

image descriptor and a point cloud descriptor to extract visual and geometric features  $\mathbf{f}_{vis}, \mathbf{f}_{geo}$  from the data. After feature extraction, we match the features by directly finding the nearest neighbor to each point in the appropriate feature space. Consequently, we obtain a set of visual correspondences  $C_{vis}$  and a set of geometric correspondences  $C_{geo}$ . Note that, any feature descriptor can be used in our framework.

To improve the accuracy and efficiency, we filter the visual correspondences using Lowe’s ratio [35]. Given a visual correspondence pair  $\mathbf{p}, \mathbf{q}$  and the corresponding feature vectors  $\mathbf{f}_p, \mathbf{f}_q$ , we calculate the ratio as follows:

$$r_{p,q} = \frac{D(\mathbf{f}_p, \mathbf{f}_q)}{D(\mathbf{f}_p, \mathbf{f}_q^{nn2})}, \quad (1)$$

where  $D(\cdot)$  is the Euclidean distance in the feature space,  $\mathbf{f}_q$  is the nearest neighbor of  $\mathbf{f}_p$  and  $\mathbf{f}_q^{nn2}$  is the second-nearest neighbor for  $\mathbf{f}_p$ . The correspondences whose ratio exceeds a predefined threshold will be regarded as unreliable points and thus eliminated from the subsequent steps. Using this test, we can improve the inlier ratio of visual correspondences and obtain a more credible correspondence set. Note that, for matching methods such as LightGlue [34], owing to their own feature matchers, we directly use the output correspondences without the ratio test.

### 3.2 Adaptive Filter Based on Transformation Consistency

In this process, we first estimate the geometric transformation via visual correspondences and obtain assumed inliers to estimate the error distribution. An

adaptive threshold is then calculated through the estimated distribution. Using the threshold, we filter the geometric correspondences and extract the credible ones to obtain the set  $C$ , which contains the valid information and is used to achieve accurate geometric fitting.

**Estimation of the error distribution.** By mapping the visual correspondences into 3D points using the camera intrinsic matrix, we can turn the set  $C_{vis}$  into a 3D correspondence set. Then, we use RANSAC to estimate a roughly accurate geometric transformation  $\mathbf{T}$  between two point clouds via the set  $C_{vis}$ . Given the estimated transformation  $\mathbf{T}$  and a matching pair  $\mathbf{p}, \mathbf{q}$ , we calculate the Euclidean distance error  $d_T$  as follows:

$$d_T = \|\mathbf{T}(\mathbf{p}) - \mathbf{q}\|, \quad (2)$$

where  $\mathbf{T}(\mathbf{p})$  implies applying geometric transformation  $\mathbf{T}$  to 3D point  $\mathbf{p}$ . For inliers conform to the transformation  $\mathbf{T}$ , we assume that the errors in the  $x$ -axis,  $y$ -axis and  $z$ -axis satisfy independent identical Gaussian distributions  $N(0, \sigma^2)$  and have same variance. Therefore, the distribution of the Euclidean distance error  $d_T$  can be regard as a Chi-square distribution:

$$d_T^2 = d_x^2 + d_y^2 + d_z^2, \quad \frac{d_x^2 + d_y^2 + d_z^2}{\sigma^2} \sim \chi^2(3). \quad (3)$$

To estimate the variance  $\sigma^2$ , we obtain assumed inliers in  $C_{vis}$  using the inlier threshold  $t_{in}$ , which has also been used in the RANSAC transformation estimation. An inlier set  $C_{vis}^{in}$  can be obtained with the assumed inliers:

$$C_{vis}^{in} = \{\mathbf{p}_i, \mathbf{q}_i \in C_{vis} \mid \|\mathbf{T}(\mathbf{p}_i) - \mathbf{q}_i\| \leq K t_{in}\}. \quad (4)$$

where the multiplier  $K$  is introduced to tolerate the rough transformation estimation. When the visual correspondences are weak, the estimated transformation is likely to be incorrect. In this case, the assumed inliers obtained by the RANSAC threshold  $t_{in}$  can not reflect the real estimation error, and the estimated variance will be lower than the true value. For real-world data, making the inlier threshold of variance estimation larger than the RANSAC threshold can improve the robustness. After that, we use the set  $C_{vis}^{in}$  as a sample for moment estimation:

$$\hat{\sigma}^2 = \frac{1}{3|C_{vis}^{in}|} \sum_i^{|C_{vis}^{in}|} \|\mathbf{T}(\mathbf{p}_i) - \mathbf{q}_i\|^2. \quad (5)$$

**Calculation of the adaptive threshold.** It's obvious that outliers do not conform to the geometric transformation, and thus have a considerably larger distance error than inliers. Therefore, if we have estimated the error distribution of inliers, we can regard the correspondences which have low probability of conforming to the distribution as outliers. To this end, we establish the 95% confidence interval of the estimated distribution:

$$P\left(\frac{d^2}{\sigma^2} \leq \chi_{0.95}^2(3)\right) = 0.95, \quad (6)$$

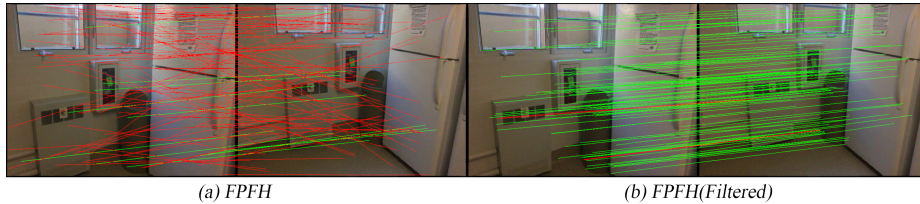


**Fig. 3:** Correspondence estimation result yielded by our proposed method. The green lines denote the correct correspondences, and the red lines denote the incorrect correspondences. For better visualization, we randomly sample parts of matches to draw the lines. The result shows that the processed correspondences have high inlier ratio.

where  $\chi_{0.95}^2(3)$  is the 0.95 quantile of Chi-square distribution. The correspondences whose distance error is within the confidence interval have a high probability of conforming to the error distribution, and are likely to be the inliers. Therefore, we can calculate the adaptive threshold  $\epsilon$ :

$$\epsilon = \sqrt{\sigma^2 \chi_{0.95}^2(3)}. \quad (7)$$

This threshold can be used to find the correspondences with high transformation consistency and inlier probability. Since the threshold is calculated from the error distribution, the value of threshold depends on the quality of visual correspondences. Weak visual correspondences usually result in rough transformation estimation and large error distribution. In this case, a loose threshold will be calculated. On the contrary, strong visual correspondences usually have a minor error distribution and result in a strict threshold. Therefore, the designed threshold is adaptive that it can vary suitably with different situations, which is important for the robustness.

**Extraction of credible geometric correspondences.** Using the threshold  $\epsilon$ , we can apply a test to determine the geometric correspondences that conform to the estimated distribution:

$$C_{geo}^{in} = \{\mathbf{p}_i, \mathbf{q}_i \in C_{geo} \mid \|\mathbf{T}(\mathbf{p}_i) - \mathbf{q}_i\| \leq \epsilon\}. \quad (8)$$

After filtering, the survived geometric correspondences will have a distance error within the confidence interval. This indicates that the corresponding transformation of the survived correspondences is likely to be consistent with the estimated transformation  $\mathbf{T}$ , and thus those correspondences are more likely to be the correct matches. Therefore, we can extract correspondences with high transformation consistency, and effectively remove the incorrect matches. The filter results are shown in Fig. 3. This fusion strategy aims to overcome the weakness of each type of feature. We leverage the high accuracy of visual correspondences to find credible geometric correspondences and remove the outliers. Meanwhile, the abundant information extracted from geometric correspondences can significantly improve the registration performance. Therefore, we can effectively leverage the advantages of both two types of features, and obtain sufficient and



credible correspondences of two point clouds. To avoid the negative effect of wrong transformation estimation, the filter will be skipped when there are few visual correspondences or when there are almost no survived correspondences after filtering. Finally, we merge the visual correspondence set  $C_{vis}^{in}$  and the geometric correspondence set  $C_{geo}^{in}$  to obtain the final set  $C$ , which contains the valid information in both visual and geometric correspondences:

$$C = C_{vis}^{in} + C_{geo}^{in}. \quad (9)$$

### 3.3 Geometric Fitting

Using the set  $C$ , we re-estimate the transformation  $\mathbf{T} \in SE(3)$  that minimizes the error between the aligned correspondences in set  $C$  as follows:

$$\mathbf{T} = \underset{\mathbf{T}' \in SE(3)}{\operatorname{argmin}} \frac{1}{|C|} \sum_{(\mathbf{p}, \mathbf{q}, w) \in C} w_i \|\mathbf{T}'(\mathbf{p}_i) - \mathbf{q}_i\|^2, \quad (10)$$

where  $w$  is a weight computed using the feature distance of  $\mathbf{p}, \mathbf{q}$ . This equation can be solved as a weighted Procrustes problem [25, 30, 46] and has been used in BYOC [19] and GeoTransformer [37]. According to BYOC and relevant studies [18, 51, 57], we adopt the same randomized optimization to improve robustness.

To fully exploit the high-quality correspondences extracted by our method, we apply post-refinement after solving the transformation, which is a typical approach [4, 13]. We use the estimated transformation  $\mathbf{T}$  to determine the inliers in the set  $C$  and construct the assumed inlier set  $C_{in}$ :

$$C_{in} = \{\mathbf{p}_i, \mathbf{q}_i \in C \mid \|\mathbf{T}(\mathbf{p}_i) - \mathbf{q}_i\| \leq t_{in}\}. \quad (11)$$

Subsequently, we use the set  $C_{in}$  to recompute the transformation in a least-squares manner and obtain a refined result. This process can be repeated to obtain more accurate result. Owing to the high-quality correspondences extracted by our method, we can achieve fine registration via a few iterations, which does not increase computation significantly.

## 4 Experiment

### 4.1 Experimental Settings

**Datasets.** We follow the setting in BYOC [19] and use the indoor RGB-D dataset ScanNet [14] for evaluation. Notably, it contains 1513 scenes and is also used as the evaluation dataset for UR&R [18], LLT [51], and PointMBF [57]. Similar to the case of BYOC, we generate view pairs by sampling image pairs that are 20 frames apart. In addition, a much smaller RGB-D dataset 3DMatch [58] with 101 scenes is used. As 3DMatch is a well-known dataset in point cloud registration tasks and has been used in several studies [2, 11, 37], we selected it as the training dataset for the learning-based baseline methods.

**Table 1:** Point cloud registration on ScanNet. Ours(No Learning) denotes the no learning version of RGBD-Glue which uses SIFT and FPFH as descriptors.

	Rotation(deg)					Translation(cm)					Chamfer(mm)				
	Accuracy $\uparrow$		Error $\downarrow$			Accuracy $\uparrow$		Error $\downarrow$			Accuracy $\uparrow$		Error $\downarrow$		
	5	10	45	Mean	Med.	5	10	25	Mean	Med.	1	5	10	Mean	Med.
FCGF [12]+DGR [11]	84.0	88.7	94.1	10.9	1.2	64.1	77.5	85.1	22.4	3.4	73.6	83.1	86.4	15.8	0.3
FCGF [12]+PointDSC [2]	93.9	98.2	99.0	3.4	1.5	62.4	90.9	97.6	7.6	4.1	84.5	96.6	97.8	5.4	0.3
FCGF [12]+MAC [59]	95.3	98.2	99.1	3.1	1.3	67.3	88.5	97.1	7.4	3.5	82.4	95.1	97.1	5.9	0.2
GeoTransformer [37]	92.4	95.7	97.8	4.9	1.1	74.0	89.8	96.0	9.4	2.9	85.1	94.6	96.2	6.7	0.2
BYOC [19]	66.5	85.2	97.8	7.4	3.3	30.7	57.6	88.9	16.0	8.2	54.1	82.8	89.5	9.5	0.9
UR&R [18]	87.6	93.1	98.3	4.3	1.0	69.2	84.0	93.8	9.5	2.8	79.7	91.3	94.0	7.2	0.2
UR&R(RGBD)	87.6	93.7	98.8	3.8	1.1	67.5	83.8	94.6	8.5	3.0	78.6	91.7	94.6	6.5	0.2
LLT [51]	93.4	96.5	98.8	3.0	0.9	76.9	90.2	96.7	6.4	2.4	86.4	95.1	96.8	5.3	0.1
PointMBF [57]	94.6	97.0	98.7	3.0	0.8	81.0	92.0	97.1	6.2	2.1	91.3	96.6	97.4	4.9	0.1
Ours(No Learning)	89.3	91.6	95.8	7.2	<b>0.7</b>	81.3	87.3	92.0	13.7	1.7	85.1	90.1	91.7	13.4	<b>0.1</b>
Ours	<b>99.1</b>	<b>99.5</b>	<b>99.7</b>	<b>1.3</b>	<b>0.7</b>	<b>92.3</b>	<b>98.2</b>	<b>99.4</b>	<b>3.0</b>	<b>1.6</b>	<b>96.7</b>	<b>99.2</b>	<b>99.5</b>	<b>3.5</b>	<b>0.1</b>

**Metrics.** We use the rotation error, the translation error and the chamfer distance to evaluate registration performance, report mean, median and accuracy under different thresholds, as in previous studies [18, 19, 51, 57]. We report the translation error in centimeters, the rotation error in degrees and the chamfer distance in millimeters.

**Baseline Methods.** We compare our method with recent studies on correspondence estimation, including DGR [11], PointDSC [2], GeoTransformer [37], and MAC [59]. For GeoTransformer, we use its own feature extractor, and for the others, we use FCGF [12] to extract geometric features. The pretrained models used for DGR, PointDSC, GeoTransformer and FCGF are trained on 3DMatch dataset. Additionally, we compare our method with recent feature fusion based methods, including UR&R [18], BYOC [19], LLT [51], PointMBF [57], and an RGB-D version of UR&R. Similarly, these methods are evaluated using models trained on 3DMatch dataset.

**Implementation Details.** As RGBD-Glue is a general framework that is compatible with any feature descriptor, we evaluate our method using different descriptors, including SIFT [35], LightGlue [34], FPFH [41], and FCGF [12]. SIFT and FPFH are hand-crafted descriptors, FCGF is a learning-based descriptor, and LightGlue is a learning-based feature extractor and matcher. Experiments with more visual features can be found in supplementary material. In our experiment, we use LightGlue and FCGF to achieve the best performance. We also use SIFT and FPFH to evaluate our method without any learning, which is listed as a no-learning version. Moreover, we downsample the point clouds with a voxel size of 2.5 cm, which is suitable for indoor datasets [12, 37, 52].

## 4.2 Point Cloud Registration

As shown in Tab. 1, our proposed method achieves a state-of-the-art performance in all the metrics. Without learning, the performance of our method is comparable to that of learning-based methods. And by using learning-based feature descriptors, our method achieves a significant performance improvement.

**Table 2:** Point cloud registration with different descriptors and settings. Add Corr. denotes the use of both  $C_{vis}^{in}$  and  $C_{geo}^{in}$  correspondence sets instead of only  $C_{geo}^{in}$  correspondence set in geometric fitting. Post Refi. denotes the application of post-refinement in geometric fitting.

Visual Feature	Add Corr.	Post Refi.	Rotation(deg)					Translation(cm)					Chamfer(mm)				
			Accuracy $\uparrow$			Error $\downarrow$		Accuracy $\uparrow$			Error $\downarrow$		Accuracy $\uparrow$			Error $\downarrow$	
			5	10	45	Mean	Med.	5	10	25	Mean	Med.	1	5	10	Mean	Med.
<b>Only Visual Feature</b>																	
SIFT	-		76.5	85.6	95.1	10.0	2.0	44.5	68.5	85.6	20.9	5.8	62.2	81.4	86.6	15.2	0.5
LightGlue	-		97.1	99.1	99.8	1.6	0.9	74.7	92.3	98.8	4.6	2.7	87.1	97.5	98.8	4.2	0.2
<b>FPFH + Visual Feature</b>																	
-			14.0	40.5	88.2	23.5	12.3	2.7	10.7	41.6	53.4	30.2	3.7	22.3	39.4	40.0	14.5
SIFT			84.7	89.8	96.1	7.4	1.1	67.9	81.6	90.3	14.8	2.9	77.0	87.8	90.6	11.1	0.2
LightGlue			98.7	99.3	99.6	1.6	0.8	88.3	97.4	99.3	3.9	2.0	94.8	98.9	99.3	3.8	0.1
SIFT	$\checkmark$		84.0	89.4	96.2	7.5	1.1	68.9	82.1	90.2	14.8	2.8	77.2	87.8	90.5	11.5	0.2
SIFT	$\checkmark$	$\checkmark$	89.3	91.6	95.8	7.2	0.7	81.3	87.3	92.0	13.7	1.7	85.1	90.1	91.7	13.4	0.1
<b>FCGF + Visual Feature</b>																	
-			76.0	89.0	96.9	8.3	2.7	33.5	64.0	85.6	19.8	7.1	56.0	80.2	86.6	14.7	0.8
SIFT			88.6	92.9	97.3	5.4	1.0	73.6	86.4	93.0	11.3	2.6	82.6	91.1	93.3	8.9	0.2
LightGlue			98.8	99.4	99.7	1.4	0.8	88.8	97.7	99.4	3.5	2.0	95.1	99.1	99.4	3.5	0.1
LightGlue	$\checkmark$		99.0	99.4	99.7	1.3	0.7	90.0	97.9	99.4	3.3	1.9	95.5	99.2	99.4	3.5	0.1
LightGlue	$\checkmark$	$\checkmark$	99.1	99.5	99.7	1.3	0.7	92.3	98.2	99.4	3.0	1.6	96.7	99.2	99.5	3.5	0.1

Compared with correspondence estimation methods, our method outperforms recent learning-based methods, such as PointDSC [2] and GeoTransformer [37]. By effectively leveraging the advantages of both visual and geometric features, our method achieves the best performance among feature fusion methods. In particular, our method achieves a high accuracy under strict thresholds and an accuracy of approximately 100% under loose thresholds, which indicates its robustness. In addition, by comparing our method with the previous state-of-the-art method PointMBF [57], our fusion strategy is effective and can be a better strategy than PointMBF’s multi-scale bidirectional fusion. Moreover, our method is a general framework compatible with any feature descriptor and can be learning-free. Therefore, our method is more flexible for handling various RGB-D point cloud registration tasks.

### 4.3 Ablations

We conduct comprehensive ablation studies to demonstrate the effectiveness of our proposed method. The method is evaluated using the ScanNet [14] dataset. To make further demonstration, we provide more experiments in the supplementary material.

**Visual features vs. geometric features.** We observe that visual features can easily achieve a high inlier ratio. By performing the ratio test or using the learning-based matcher, the visual feature correspondences can achieve a high accuracy under both loose and strict thresholds. This may be because of the abundant texture information of visual features, which renders them more distinctive than geometric features. However, this does not imply that visual

**Table 3:** Inlier ratio and amount of correspondence estimation. We filter the original geometric feature correspondences using our method and find inliers under different thresholds without Add Corr. In point cloud correspondence estimation, 10 cm is a typical threshold [2, 37]. Filter recall denotes the percentage of data processed by filter.

Visual Feature	Mean Inlier Ratio(%)			Mean Inlier Amount			Filter Recall
	10 cm	5 cm	2.5 cm	10 cm	5 cm	2.5 cm	
<b>Only Visual Feature</b>							
SIFT	55.7	48.5	37.2	65	57	45	-
LightGlue	93.3	84.8	65.0	239	219	171	-
<b>FPFH + Visual Feature</b>							
-	11.5	7.2	3.8	693	424	217	-
SIFT	76.1	48.6	23.5	599	404	210	96.0
LightGlue	96.9	80.9	45.1	380	340	207	99.4
<b>FCGF + Visual Feature</b>							
-	50.1	34.9	15.2	3502	2383	1013	-
SIFT	85.8	60.0	25.5	3127	2254	973	96.0
LightGlue	97.5	82.3	41.5	2303	1973	968	99.4

features are better in all cases. Because of varying viewpoints, different lighting, and weak texture, not every pixel can be extracted with a valid local feature for matching, and generating sufficient inliers using only visual features is unreliable. By contrast, geometric features have different challenges, such as ambiguous and repetitive structures, and the low inlier ratio is usually a more serious problem. As shown in Tab. 2 and Tab. 3, although most geometric correspondences are outliers, there are still quite a number of inliers that can achieve accurate registration after filtering. Therefore, we use a looser fusion to effectively leverage each feature’s advantages.

**Performance of feature combination.** As shown in Tab. 2, our method shows a significant improvement compared with using individual geometric features. We observe that using visual features particularly LightGlue [34], can achieve a high registration accuracy. However, when visual features are combined with FPFH [41], which exhibits a very low accuracy in correspondence estimation, a better performance can be achieved. Meanwhile, when visual features are combined with a superior descriptor FCGF [12], a much better performance can be achieved compared with using only visual or geometric features. More detailed, as shown in Tab. 3, our method can allow the filtered geometric correspondences to achieve high inlier ratio and maintain most of the inliers under the 2.5 cm threshold. With high-quality visual correspondences, our method can fully extract the valid information from geometric correspondences. On the contrary, when visual correspondences are weak, our method can avoid incorrect filtering and retain most valid information in geometric correspondences, which prevents a worse performance. The results indicate that compared with other fusion strategies [51, 57], our proposed strategy can sufficiently leverage the valid information and avoid the adverse effects caused by the different limitations of

**Table 4:** Registration accuracy, mean inlier ratio and filter recall under different  $K$  values. Add Corr. and Post Refi. are both used.

$K$	Rotation(deg)			Translation(cm)			Chamfer(mm)			Inlier Ratio(%)			Filter Recall
	5	10	45	5	10	25	1	5	10	10	5	2.5	
<b>FPFH + SIFT</b>													
1	81.4	85.9	93.7	68.5	77.9	85.3	74.9	82.2	85.0	81.0	73.7	50.5	81.5
3	88.2	91.0	95.7	79.4	85.9	90.9	84.0	89.0	90.7	82.7	63.7	35.4	92.6
5	89.3	91.6	95.8	81.3	87.3	92.0	85.1	90.1	91.7	76.1	51.2	27.2	96.0
7	90.1	92.3	96.1	81.7	87.7	92.1	85.4	90.4	92.2	66.7	42.3	22.3	97.5
<b>FCGF + LightGlue</b>													
1	99.0	99.4	99.6	90.9	98.0	99.3	95.9	99.0	99.3	98.6	91.4	56.2	99.3
3	99.1	99.5	99.7	92.3	98.2	99.4	96.7	99.2	99.5	97.5	83.0	44.7	99.4
5	99.1	99.5	99.7	92.6	98.1	99.5	96.8	99.2	99.4	96.4	79.2	40.6	99.5
7	99.2	99.5	99.7	92.3	98.1	99.5	96.7	99.2	99.4	95.5	76.1	38.0	99.5

the two modalities. Moreover, as mentioned in Sec. 3.2, filter will be skipped in some cases. Therefore, we additionally calculate the percentage of data that has been processed by the filter as filter recall. The results demonstrate that our proposed filter has effectively removed outliers in most of the data.

**Effect of  $K$ .** As mentioned in Sec. 3.2, we use a multiplier  $K$  to magnify the threshold. This is because the visual correspondences may result in inaccurate transformation estimation when they are weak. Therefore, we set  $K$  to reduce the constraints of visual feature for better robustness. The results are shown in Tab. 4, which indicates that increasing  $K$  results in better performance. More detailed, increasing  $K$  can improve the filter’s performance when facing low-quality visual correspondences. Better robustness and higher filter recall can be obtained by increasing  $K$ . However, increasing  $K$  will also reduce the inlier ratio, and cause slight performance deterioration when the visual correspondences are strong. Therefore, it’s important to set a suitable  $K$  balancing the robustness and accuracy. We notice that our method is insensitive to the variation of  $K$  when  $K$  exceeds a specific value. Therefore, we believe a fixed value set respectively for hand-crafted and learning-based visual features can handle general cases, and higher value is needed when the visual correspondences are quite weak. In our experiments, we set  $K = 3$  for learning-based visual feature such as LightGlue [34], and  $K = 5$  for hand-crafted visual feature such as SIFT [35].

**Effect of post-refinement.** As mentioned in Sec. 3.3, we obtain the assumed inliers in correspondences via the estimated transformation and use the least-squares method to obtain better results. The post-refinement performance depends primarily on the accuracy of the preceding geometric fitting. Using our proposed method, we extract high-quality correspondences. Therefore, the transformation estimated before post-refinement is relatively accurate, and the assumed inliers are highly likely to be the true inliers. This shows that better registration results can be obtained. As shown in Tab. 2, the post-refinement improves the performance of our method in all the metrics.

**Table 5:** Registration accuracy and median error under large frame spacing. We use 40 and 60 frames apart instead of 20 frames apart to evaluate the performance under large frame spacing. We use FCGF [12] and LightGlue [34] for our method’s evaluation and compare the performance with only LightGlue [34], GeoTransformer [37] and PointMBF [57]. Ours(No Post Refi.) denotes the version without post refinement.

	Rotation(deg)				Translation(cm)				Chamfer(mm)			
	Accuracy $\uparrow$			Error $\downarrow$	Accuracy $\uparrow$			Error $\downarrow$	Accuracy $\uparrow$			Error $\downarrow$
	5	10	45	Med.	5	10	25	Med.	1	5	10	Med.
<b>40 frames apart</b>												
LightGlue [34]	87.1	93.4	<b>97.0</b>	1.5	53.0	76.9	92.3	4.6	66.9	87.3	91.8	0.4
GeoTransformer [37]	75.7	83.0	90.1	1.9	49.3	70.5	83.0	5.1	61.8	78.9	82.2	0.5
PointMBF [57]	71.1	79.1	89.8	1.8	48.4	65.7	79.8	5.3	63.1	77.0	80.7	0.4
Ours(No Post Refi.)	93.2	<b>95.6</b>	96.6	1.1	71.9	88.5	<b>95.1</b>	3.0	82.1	<b>93.5</b>	<b>94.8</b>	<b>0.2</b>
Ours	<b>94.3</b>	95.5	96.6	<b>1.0</b>	<b>76.1</b>	<b>90.1</b>	<b>95.1</b>	<b>2.6</b>	<b>85.2</b>	<b>93.5</b>	<b>94.8</b>	<b>0.2</b>
<b>60 frames apart</b>												
LightGlue [34]	71.3	80.3	<b>89.4</b>	2.3	37.3	58.9	78.0	7.5	48.8	70.6	76.2	1.1
GeoTransformer [37]	56.4	64.8	76.0	3.5	32.5	51.7	64.7	9.4	42.0	58.8	63.0	1.9
PointMBF [57]	45.4	55.8	73.3	6.6	25.9	38.4	55.1	18.8	36.2	50.8	55.9	4.5
Ours(No Post Refi.)	80.8	84.9	88.3	1.5	54.7	73.6	84.0	4.3	63.8	79.8	82.8	<b>0.4</b>
Ours	<b>82.6</b>	<b>86.0</b>	88.1	<b>1.4</b>	<b>58.8</b>	<b>75.8</b>	<b>84.2</b>	<b>3.9</b>	<b>67.2</b>	<b>80.3</b>	<b>83.1</b>	<b>0.4</b>

**Registration under large frame spacing.** We notice that 20 frames apart is less challenging, making the improvement of our method not obvious. Therefore, we evaluate the registration performance under larger frame spacing to further demonstrate our method’s effectiveness. Larger frame spacing will cause lower overlap, which brings great challenge to both visual and geometric feature matching. We compare our method with LightGlue [34], GeoTransformer [37] and PointMBF [57]. The results are shown in Tab. 5, which indicates that our method has significantly better performance. Besides, by combining visual and geometric information effectively, our method can achieve considerable improvement compared with only LightGlue. Moreover, the post refinement still have great performance under large frame spacing, which demonstrates the high quality of the correspondences extracted by our method.

## 5 Conclusion

A general framework RGBD-Glue for RGB-D point cloud registration is proposed in this paper. Differ from other fusion works, we use an explicit filter based on transformation consistency to achieve a looser fusion and design an adaptive threshold to extract more valid information, which bring our method better performance and robustness. Besides, the applicability of different descriptors renders our proposed method flexible to various registration tasks. The experiments show that our method achieves a better performance compared with using individual feature, and demonstrates a state-of-the-art performance. Furthermore, our method can be extended to other RGB-D based tasks, and exploiting more information from RGB images to improve correspondence estimation is still a worth exploring task. We will make further research in our future work.

## References

1. Ao, S., Hu, Q., Yang, B., Markham, A., Guo, Y.: Spinnet: Learning a general surface descriptor for 3d point cloud registration. In: Proceedings of the IEEE/CVF conference on computer vision and pattern recognition. pp. 11753–11762 (2021) [1](#)
2. Bai, X., Luo, Z., Zhou, L., Chen, H., Li, L., Hu, Z., Fu, H., Tai, C.L.: Pointdsc: Robust point cloud registration using deep spatial consistency. In: Proceedings of the IEEE/CVF Conference on Computer Vision and Pattern Recognition. pp. 15859–15869 (2021) [4](#), [9](#), [10](#), [11](#), [12](#)
3. Bai, X., Luo, Z., Zhou, L., Fu, H., Quan, L., Tai, C.L.: D3feat: Joint learning of dense detection and description of 3d local features. In: Proceedings of the IEEE/CVF conference on computer vision and pattern recognition. pp. 6359–6367 (2020) [1](#), [4](#)
4. Barath, D., Matas, J.: Graph-cut ransac. In: Proceedings of the IEEE conference on computer vision and pattern recognition. pp. 6733–6741 (2018) [9](#)
5. Bay, H., Tuytelaars, T., Van Gool, L.: Surf: Speeded up robust features. In: Computer Vision—ECCV 2006: 9th European Conference on Computer Vision, Graz, Austria, May 7–13, 2006. Proceedings, Part I 9. pp. 404–417. Springer (2006) [4](#)
6. Besl, P.J., McKay, N.D.: Method for registration of 3-d shapes. In: Sensor fusion IV: control paradigms and data structures. vol. 1611, pp. 586–606. Spie (1992) [4](#)
7. Chen, H., Luo, Z., Zhou, L., Tian, Y., Zhen, M., Fang, T., Mckinnon, D., Tsin, Y., Quan, L.: Aspanformer: Detector-free image matching with adaptive span transformer. In: European Conference on Computer Vision. pp. 20–36. Springer (2022) [4](#)
8. Chen, X., Lin, K.Y., Wang, J., Wu, W., Qian, C., Li, H., Zeng, G.: Bi-directional cross-modality feature propagation with separation-and-aggregation gate for rgb-d semantic segmentation. In: European Conference on Computer Vision. pp. 561–577. Springer (2020) [5](#)
9. Chen, Z., Sun, K., Yang, F., Tao, W.: Sc2-pcr: A second order spatial compatibility for efficient and robust point cloud registration. In: Proceedings of the IEEE/CVF Conference on Computer Vision and Pattern Recognition. pp. 13221–13231 (2022) [4](#)
10. Cho, M., Lee, K.M.: Progressive graph matching: Making a move of graphs via probabilistic voting. In: 2012 IEEE Conference on Computer Vision and Pattern Recognition. pp. 398–405. IEEE (2012) [4](#)
11. Choy, C., Dong, W., Koltun, V.: Deep global registration. In: Proceedings of the IEEE/CVF conference on computer vision and pattern recognition. pp. 2514–2523 (2020) [2](#), [4](#), [9](#), [10](#)
12. Choy, C., Park, J., Koltun, V.: Fully convolutional geometric features. In: Proceedings of the IEEE/CVF international conference on computer vision. pp. 8958–8966 (2019) [1](#), [4](#), [10](#), [12](#), [14](#), [22](#)
13. Chum, O., Matas, J., Kittler, J.: Locally optimized ransac. In: Pattern Recognition: 25th DAGM Symposium, Magdeburg, Germany, September 10–12, 2003. Proceedings 25. pp. 236–243. Springer (2003) [9](#)
14. Dai, A., Chang, A.X., Savva, M., Halber, M., Funkhouser, T., Nießner, M.: Scannet: Richly-annotated 3d reconstructions of indoor scenes. In: Proceedings of the IEEE conference on computer vision and pattern recognition. pp. 5828–5839 (2017) [3](#), [9](#), [11](#), [21](#)
15. Dai, L., Liu, Y., Ma, J., Wei, L., Lai, T., Yang, C., Chen, R.: Ms2dg-net: Progressive correspondence learning via multiple sparse semantics dynamic graph. In: Proceed-

- ings of the IEEE/CVF Conference on Computer Vision and Pattern Recognition. pp. 8973–8982 (2022) [4](#)
16. DeTone, D., Malisiewicz, T., Rabinovich, A.: Superpoint: Self-supervised interest point detection and description. In: Proceedings of the IEEE conference on computer vision and pattern recognition workshops. pp. 224–236 (2018) [4](#), [19](#)
  17. Dusmanu, M., Rocco, I., Pajdla, T., Pollefeys, M., Sivic, J., Torii, A., Sattler, T.: D2-net: A trainable cnn for joint detection and description of local features. arXiv preprint arXiv:1905.03561 (2019) [4](#)
  18. El Banani, M., Gao, L., Johnson, J.: Unsuperviseddr&r: Unsupervised point cloud registration via differentiable rendering. In: Proceedings of the IEEE/CVF Conference on Computer Vision and Pattern Recognition. pp. 7129–7139 (2021) [2](#), [3](#), [4](#), [5](#), [9](#), [10](#)
  19. El Banani, M., Johnson, J.: Bootstrap your own correspondences. In: Proceedings of the IEEE/CVF International Conference on Computer Vision. pp. 6433–6442 (2021) [2](#), [3](#), [4](#), [5](#), [9](#), [10](#), [22](#)
  20. Enqvist, O., Josephson, K., Kahl, F.: Optimal correspondences from pairwise constraints. In: 2009 IEEE 12th international conference on computer vision. pp. 1295–1302. IEEE (2009) [4](#)
  21. Fischler, M.A., Bolles, R.C.: Random sample consensus: a paradigm for model fitting with applications to image analysis and automated cartography. Communications of the ACM **24**(6), 381–395 (1981) [4](#)
  22. Geiger, A., Lenz, P., Urtasun, R.: Are we ready for autonomous driving? the kitti vision benchmark suite. In: 2012 IEEE conference on computer vision and pattern recognition. pp. 3354–3361. IEEE (2012) [5](#), [22](#)
  23. Glent Buch, A., Yang, Y., Kruger, N., Gordon Petersen, H.: In search of inliers: 3d correspondence by local and global voting. In: Proceedings of the IEEE Conference on computer vision and pattern recognition. pp. 2067–2074 (2014) [4](#)
  24. Gojcic, Z., Zhou, C., Wegner, J.D., Guibas, L.J., Birdal, T.: Learning multiview 3d point cloud registration. In: Proceedings of the IEEE/CVF conference on computer vision and pattern recognition. pp. 1759–1769 (2020) [2](#)
  25. Gower, J.C.: Generalized procrustes analysis. Psychometrika **40**, 33–51 (1975) [9](#)
  26. Gupta, S., Girshick, R., Arbeláez, P., Malik, J.: Learning rich features from rgb-d images for object detection and segmentation. In: Computer Vision–ECCV 2014: 13th European Conference, Zurich, Switzerland, September 6–12, 2014, Proceedings, Part VII 13. pp. 345–360. Springer (2014) [5](#)
  27. Hazirbas, C., Ma, L., Domokos, C., Cremers, D.: Fusetnet: Incorporating depth into semantic segmentation via fusion-based cnn architecture. In: Computer Vision–ACCV 2016: 13th Asian Conference on Computer Vision, Taipei, Taiwan, November 20–24, 2016, Revised Selected Papers, Part I 13. pp. 213–228. Springer (2017) [5](#)
  28. Hu, W., Zhao, H., Jiang, L., Jia, J., Wong, T.T.: Bidirectional projection network for cross dimension scene understanding. In: Proceedings of the IEEE/CVF Conference on Computer Vision and Pattern Recognition. pp. 14373–14382 (2021) [5](#)
  29. Huang, S., Gojcic, Z., Usvyatsov, M., Wieser, A., Schindler, K.: Predator: Registration of 3d point clouds with low overlap. In: Proceedings of the IEEE/CVF Conference on computer vision and pattern recognition. pp. 4267–4276 (2021) [1](#), [4](#)
  30. Kabsch, W.: A solution for the best rotation to relate two sets of vectors. Acta Crystallographica Section A: Crystal Physics, Diffraction, Theoretical and General Crystallography **32**(5), 922–923 (1976) [9](#)



31. Leutenegger, S., Chli, M., Siegwart, R.Y.: Brisk: Binary robust invariant scalable keypoints. In: 2011 International conference on computer vision. pp. 2548–2555. Ieee (2011) [4](#), [19](#)
32. Li, Y., Yu, A.W., Meng, T., Caine, B., Ngiam, J., Peng, D., Shen, J., Lu, Y., Zhou, D., Le, Q.V., et al.: Deepfusion: Lidar-camera deep fusion for multi-modal 3d object detection. In: Proceedings of the IEEE/CVF Conference on Computer Vision and Pattern Recognition. pp. 17182–17191 (2022) [5](#)
33. Liang, M., Yang, B., Wang, S., Urtasun, R.: Deep continuous fusion for multi-sensor 3d object detection. In: Proceedings of the European conference on computer vision (ECCV). pp. 641–656 (2018) [5](#)
34. Lindenberger, P., Sarlin, P.E., Pollefeys, M.: Lightglue: Local feature matching at light speed. arXiv preprint arXiv:2306.13643 (2023) [4](#), [6](#), [10](#), [12](#), [13](#), [14](#), [19](#), [21](#), [22](#)
35. Lowe, D.G.: Distinctive image features from scale-invariant keypoints. International journal of computer vision **60**, 91–110 (2004) [4](#), [6](#), [10](#), [13](#)
36. Mian, A.S., Bennamoun, M., Owens, R.A.: Automatic correspondence for 3d modeling: An extensive review. International Journal of Shape Modeling **11**(02), 253–291 (2005) [4](#)
37. Qin, Z., Yu, H., Wang, C., Guo, Y., Peng, Y., Ilic, S., Hu, D., Xu, K.: Geotransformer: Fast and robust point cloud registration with geometric transformer. IEEE Transactions on Pattern Analysis and Machine Intelligence (2023) [2](#), [4](#), [5](#), [9](#), [10](#), [11](#), [12](#), [14](#), [22](#)
38. Revaud, J., Weinzaepfel, P., De Souza, C., Pion, N., Csurka, G., Cabon, Y., Humenberger, M.: R2d2: repeatable and reliable detector and descriptor. arXiv preprint arXiv:1906.06195 (2019) [4](#)
39. Rosten, E., Drummond, T.: Machine learning for high-speed corner detection. In: Computer Vision–ECCV 2006: 9th European Conference on Computer Vision, Graz, Austria, May 7–13, 2006. Proceedings, Part I 9. pp. 430–443. Springer (2006) [4](#)
40. Rublee, E., Rabaud, V., Konolige, K., Bradski, G.: Orb: An efficient alternative to sift or surf. In: 2011 International conference on computer vision. pp. 2564–2571. Ieee (2011) [4](#), [19](#)
41. Rusu, R.B., Blodow, N., Beetz, M.: Fast point feature histograms (fpfh) for 3d registration. In: 2009 IEEE international conference on robotics and automation. pp. 3212–3217. IEEE (2009) [1](#), [4](#), [10](#), [12](#)
42. Sahloul, H., Shirafuji, S., Ota, J.: An accurate and efficient voting scheme for a maximally all-inlier 3d correspondence set. IEEE Transactions on Pattern Analysis and Machine Intelligence **43**(7), 2287–2298 (2020) [4](#)
43. Sarlin, P.E., DeTone, D., Malisiewicz, T., Rabinovich, A.: Superglue: Learning feature matching with graph neural networks. In: Proceedings of the IEEE/CVF conference on computer vision and pattern recognition. pp. 4938–4947 (2020) [4](#), [19](#)
44. Segal, A., Haehnel, D., Thrun, S.: Generalized-icp. In: Robotics: science and systems. vol. 2, p. 435. Seattle, WA (2009) [4](#)
45. Serafin, J., Grisetti, G.: Nicip: Dense normal based point cloud registration. In: 2015 IEEE/RSJ International Conference on Intelligent Robots and Systems (IROS). pp. 742–749. IEEE (2015) [4](#)
46. Sorkine-Hornung, O., Rabinovich, M.: Least-squares rigid motion using svd. Computing **1**(1), 1–5 (2017) [9](#)
47. Sun, J., Shen, Z., Wang, Y., Bao, H., Zhou, X.: Loftr: Detector-free local feature matching with transformers. In: Proceedings of the IEEE/CVF conference on computer vision and pattern recognition. pp. 8922–8931 (2021) [4](#), [19](#)

48. Vora, S., Lang, A.H., Helou, B., Beijbom, O.: Pointpainting: Sequential fusion for 3d object detection. In: Proceedings of the IEEE/CVF conference on computer vision and pattern recognition. pp. 4604–4612 (2020) [5](#)
49. Wang, Q., Zhang, J., Yang, K., Peng, K., Stiefelhagen, R.: Matchformer: Interleaving attention in transformers for feature matching. In: Proceedings of the Asian Conference on Computer Vision. pp. 2746–2762 (2022) [4](#)
50. Wang, W., Neumann, U.: Depth-aware cnn for rgb-d segmentation. In: Proceedings of the European conference on computer vision (ECCV). pp. 135–150 (2018) [5](#)
51. Wang, Z., Huo, X., Chen, Z., Zhang, J., Sheng, L., Xu, D.: Improving rgb-d point cloud registration by learning multi-scale local linear transformation. In: European Conference on Computer Vision. pp. 175–191. Springer (2022) [2](#), [3](#), [4](#), [5](#), [9](#), [10](#), [12](#)
52. Xie, S., Gu, J., Guo, D., Qi, C.R., Guibas, L., Litany, O.: Pointcontrast: Unsupervised pre-training for 3d point cloud understanding. In: Computer Vision–ECCV 2020: 16th European Conference, Glasgow, UK, August 23–28, 2020, Proceedings, Part III 16. pp. 574–591. Springer (2020) [10](#)
53. Yang, H., Shi, J., Carlone, L.: Teaser: Fast and certifiable point cloud registration. *IEEE Transactions on Robotics* **37**(2), 314–333 (2020) [4](#)
54. Yang, J., Zhang, X., Fan, S., Ren, C., Zhang, Y.: Mutual voting for ranking 3d correspondences. *IEEE Transactions on Pattern Analysis and Machine Intelligence* (2023) [4](#)
55. Yi, K.M., Trulls, E., Lepetit, V., Fua, P.: Lift: Learned invariant feature transform. In: Computer Vision–ECCV 2016: 14th European Conference, Amsterdam, The Netherlands, October 11–14, 2016, Proceedings, Part VI 14. pp. 467–483. Springer (2016) [4](#)
56. Yu, H., Li, F., Saleh, M., Busam, B., Ilic, S.: Cofinet: Reliable coarse-to-fine correspondences for robust pointcloud registration. *Advances in Neural Information Processing Systems* **34**, 23872–23884 (2021) [2](#), [4](#), [22](#)
57. Yuan, M., Fu, K., Li, Z., Meng, Y., Wang, M.: Pointmbf: A multi-scale bidirectional fusion network for unsupervised rgb-d point cloud registration. In: Proceedings of the IEEE/CVF International Conference on Computer Vision. pp. 17694–17705 (2023) [2](#), [3](#), [4](#), [5](#), [9](#), [10](#), [11](#), [12](#), [14](#), [22](#)
58. Zeng, A., Song, S., Nießner, M., Fisher, M., Xiao, J., Funkhouser, T.: 3dmatch: Learning local geometric descriptors from rgb-d reconstructions. In: Proceedings of the IEEE conference on computer vision and pattern recognition. pp. 1802–1811 (2017) [5](#), [9](#), [21](#)
59. Zhang, X., Yang, J., Zhang, S., Zhang, Y.: 3d registration with maximal cliques. In: Proceedings of the IEEE/CVF Conference on Computer Vision and Pattern Recognition. pp. 17745–17754 (2023) [4](#), [10](#)
60. Zhao, C., Cao, Z., Li, C., Li, X., Yang, J.: Nm-net: Mining reliable neighbors for robust feature correspondences. In: Proceedings of the IEEE/CVF conference on computer vision and pattern recognition. pp. 215–224 (2019) [4](#)
61. Zhou, F., De la Torre, F.: Factorized graph matching. *IEEE transactions on pattern analysis and machine intelligence* **38**(9), 1774–1789 (2015) [4](#)

# RGBD-Glue: General Feature Combination for Robust RGB-D Point Cloud Registration (Supplementary Material)

## 1 Combination with More Visual Features

**Table S1:** Point cloud registration with more visual features. BRISK [31] and ORB [40] are hand-crafted features, SuperGlue [43] and LoFTR [47] are learning-base features. The evaluation is made on ScanNet dataset.

Visual Feature	Add Corr.	Post Refi.	Rotation(deg)					Translation(cm)					Chamfer(mm)				
			Accuracy ↑			Error ↓		Accuracy ↑			Error ↓		Accuracy ↑			Error ↓	
			5	10	45	Mean	Med.	5	10	25	Mean	Med.	1	5	10	Mean	Med.
<b>FPFH + Visual Feature</b>																	
BRISK			84.2	88.5	95.5	8.2	1.0	69.7	82.2	89.4	15.9	2.7	77.9	86.8	89.3	12.0	0.2
ORB			79.4	84.6	93.2	11.5	1.2	64.2	76.6	85.7	21.0	3.2	72.2	82.3	85.3	15.9	0.2
SuperGlue			98.8	99.4	99.6	1.6	0.8	88.1	97.6	99.4	3.7	2.0	94.4	99.0	99.4	3.5	0.1
LoFTR			99.2	99.5	99.8	1.3	0.8	89.4	98.0	99.5	3.3	1.9	95.4	99.1	99.5	3.5	0.1
<b>FCGF + Visual Feature</b>																	
BRISK			87.8	92.0	96.8	6.0	1.0	73.5	85.8	92.4	12.1	2.6	81.5	90.3	92.4	9.8	0.2
ORB			84.8	89.4	95.4	8.4	1.0	69.7	82.5	89.9	15.6	2.8	78.2	87.3	89.5	12.3	0.2
SuperGlue			98.9	99.5	99.7	1.4	0.8	88.5	98.0	99.5	3.4	2.0	94.9	99.2	99.5	3.5	0.1
LoFTR			99.1	99.5	99.8	1.3	0.8	89.6	98.1	99.6	3.2	2.0	95.5	99.3	99.5	3.5	0.1

To further demonstrate our method’s generalization and flexibility, we use BRISK [31], ORB [40], SuperGlue [43] and LoFTR [47] to make extra experiments and evaluate the registration performance on ScanNet dataset. BRISK and ORB are hand-crafted features. SuperGlue is similar with LightGlue [34] since LightGlue is based on SuperGlue, and we choose SuperPoint [16] as the feature descriptor for both two methods. LoFTR is a dense learning-based extractor which has great performance but is much more time-consuming than LightGlue. We combine those visual features with FPFH or FCGF using our proposed method and evaluate their registration performance on ScanNet dataset. The results are shown in Tab. S1.

The results show that our framework is compatible with various visual features, and better visual feature descriptor or matcher can bring better performance. For practical application, it’s easy to change the feature descriptor of our framework for the more suitable one. Benefit from this, our method is more flexible and general than other fusion methods in practical tasks.

## 2 Filter’s Performance Under Large Frame Spacing

As shown in Fig. S1, large frame spacing causes low overlap which deteriorates the performance of both visual and geometric feature matching. In this case, both

**Table S2:** Mean inlier ratio and mean inlier amount under large frame spacing. FCGF and LightGlue are used without Add Corr. Filter recall denotes the percentage of data processed by filter.

	Mean Inlier Ratio(%)			Mean Inlier Amount			Filter Recall
	10 cm	5 cm	2.5 cm	10 cm	5 cm	2.5 cm	
<b>40 frames apart</b>							
Before Filtering	32.5	20.6	8.2	2242	1411	547	-
After Filtering	91.2	70.1	30.5	1563	1232	529	96.5
<b>60 frames apart</b>							
Before Filtering	22.2	13.5	5.2	1521	918	340	-
After Filtering	78.8	56.6	22.8	1085	813	329	88.4

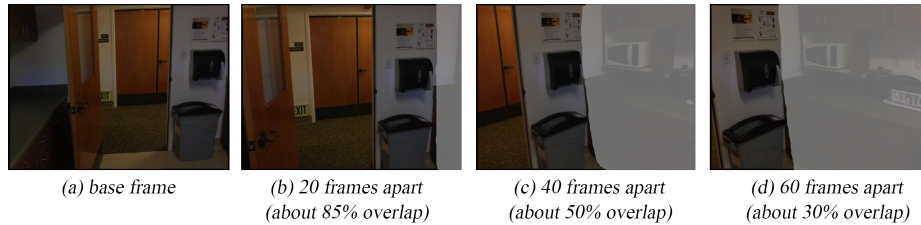


**Fig. S1:** An example of different frame spacing. We reduce the opacity of non-overlap region for better visualization. Large frame spacing causes low overlap, which brings great challenge to both visual and geometric feature matching.

visual and geometric correspondences get lower inlier ratio, which limits their registration performance. To make more detailed analysis about our method’s performance under large frame spacing, we evaluate mean inlier ratio, mean inlier amount and filter recall after the filtering.

The results are shown in Tab. S2, compare to the results under 20 frames apart in the main paper (Tab. 3), the filtered correspondences under larger frame spacing have a less significant improvement on the inlier ratio. Except the effect of worse geometric correspondences and lower filter recall (data not processed by filter usually have low inlier ratios), sparser and worse visual correspondences can cause a larger error distribution and result in lower inlier ratio improvement. However, our method can still produce high-quality correspondences even with 60 frames apart, and thus outperform other methods in registration, as shown in the main paper (Tab. 5). That demonstrates our method’s strong robustness. Furthermore, filter recall is important to the filter’s overall performance. It depends on the visual feature and the overlap of image pairs, a better or denser visual feature could improve the filter recall.

**Table S3:** Mean visual match amount and mean inlier ratio of different threshold ranges. LightGlue [34] is used as the visual feature.

Threshold Range (squared value)	Mean Match Amount	Mean Inlier Ratio(%)		
		10 cm	5 cm	2.5 cm
0 - 0.002	277	97.5	95.2	84.1
0.002 - 0.004	251	95.4	88.1	65.6
0.004 - 0.006	238	91.8	78.3	50.7
0.006 - 0.008	237	87.5	68.9	40.5
0.008 - 0.01	227	80.7	58.7	31.4

### 3 Variation of The Adaptive Threshold

To further demonstrate the effectiveness of our design, we make additional experiments to check the variation of the adaptive threshold. We generate view pairs by sampling image pairs that are 20 frames apart on ScanNet dataset, use LightGlue to extract visual correspondences and calculate the adaptive threshold. Since there are almost no data that have a squared threshold value exceed 0.01 when  $K = 3$ , we divide the squared threshold value between 0 and 0.01 into five ranges. For each range, we find the view pairs that have a calculated threshold corresponding to the range, and get their mean visual match amount. Furthermore, we map the visual correspondences into 3D correspondences and check the inliers under different distance thresholds. The comparison is made with mean match amount and mean inlier ratio, since denser and more accurate visual correspondences result in a more accurate estimation of geometric transformation.

As shown in Tab. S3, higher threshold means sparser visual correspondences and lower inlier ratio, which demonstrates that our designed adaptive threshold can change properly under different qualities of visual correspondences. When the visual correspondences are dense and accurate, the adaptive threshold will be strict to sufficiently remove the geometric outliers. On the contrary, when the visual correspondences are sparse and inaccurate, the estimated geometric transformation will get error, and the adaptive threshold will be loose to avoid removing the correct geometric correspondences. Benefit from this, our method can handle various situations without extra parameters, and can avoid the negative effect of weak visual feature. Using our designed adaptive threshold, the filter can fully extract valid information from the geometric correspondences when visual correspondences are strong, and can preserve most valid information when visual correspondences are weak, which avoids a worse registration performance than individual feature.

### 4 Point Cloud Registration on 3DMatch Dataset

Compare to ScanNet [14] dataset, 3DMatch [58] dataset is a much smaller indoor RGB-D dataset which contains 101 scenes. Our experiments in the main

**Table S4:** Point cloud registration on 3DMatch dataset. Ours(No Learning) denotes the no learning version of RGBD-Glue which uses SIFT and FPFH as descriptors.

	Rotation(deg)				Translation(cm)				Chamfer(mm)			
	Accuracy $\uparrow$		Error $\downarrow$		Accuracy $\uparrow$		Error $\downarrow$		Accuracy $\uparrow$		Error $\downarrow$	
	5	10	45	Med.	5	10	25	Med.	1	5	10	Med.
LightGlue	92.8	97.5	<b>99.2</b>	1.3	55.7	79.9	95.2	4.4	67.7	90.3	94.2	0.5
FCGF	64.4	81.3	92.3	3.4	26.6	52.2	76.9	9.3	40.3	68.6	75.6	1.6
GeoTransformer	89.9	93.8	96.6	1.3	61.4	84.4	93.2	4.0	75.1	90.4	92.0	0.4
PointMBF	86.9	91.7	96.3	1.2	63.7	82.3	91.9	3.5	75.0	89.1	91.5	0.3
Ours(No Learning)	84.1	86.3	91.3	1.1	64.7	79.2	85.4	3.2	71.5	82.2	84.5	0.3
Ours	<b>96.3</b>	<b>98.3</b>	98.7	<b>1.0</b>	<b>73.1</b>	<b>91.2</b>	<b>97.1</b>	<b>2.9</b>	<b>83.3</b>	<b>94.6</b>	<b>96.2</b>	<b>0.2</b>

paper follow the setting of BYOC [19] to use ScanNet dataset for evaluation. However, 3DMatch dataset is also a commonly used dataset for point cloud registration evaluation [12, 37, 56], and has been used as the training dataset in our main paper. Therefore, we provide extra experiments on 3DMatch dataset to further demonstrate our method’s effectiveness. We compare our method with LightGlue [34], FCGF [12], GeoTransformer [37] and PointMBF [57], evaluate registration accuracy and error. Moreover, we generate view pairs by sampling image pairs that are 40 frames apart, which can make the registration more challenging.

As shown in Tab. S4, our method achieves the best performance. Using our proposed feature combination framework, we get significantly better performance than using only LightGlue or FCGF. Besides, without any learning, our method can still achieve a great performance and can be comparable to the most advanced learning-based methods.

## 5 Filter’s Performance on Outdoor Dataset

To further demonstrate our method’s effectiveness and generalization, we make extra experiments on KITTI odometry dataset [22], which is a commonly used outdoor dataset. We use sequences 8-10 for evaluation, compare the mean inlier ratio and the mean inlier amount under different thresholds. Besides, since KITTI dataset provides LIDAR point clouds instead of depth images and the view of RGB camera is much smaller than the view of LIDAR, we remove the points that are behind the camera and the points that are not located in image after the mapping, as shown in Fig. S2. In this experiment, we use FCGF as the geometric feature extractor and LightGlue as the visual feature extractor, and the model pretrained on KITTI dataset is used for FCGF. For outdoor dataset, we downsample the point clouds with a voxel size of 0.3 m, which is a common setting [12, 37].

The results are shown in Tab. S5, which indicate that our framework effectively improve the inlier ratio although the improvement is less than the

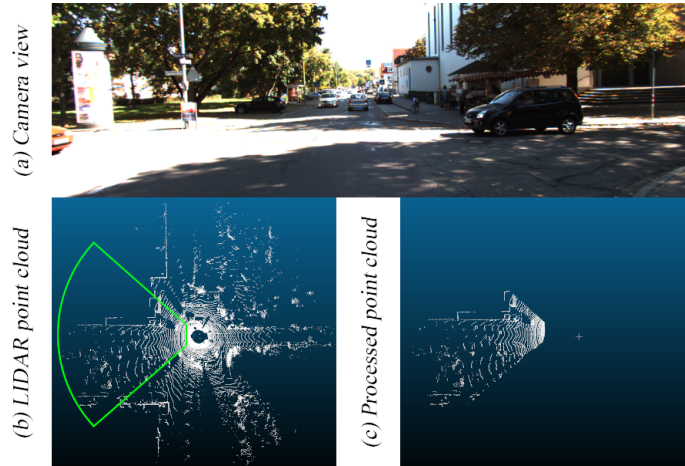


**Fig. S2:** To unified the view of camera and LIDAR, we remove the LIDAR points which are behind the camera or are not located in the camera’s field of view. As an example, we mark the points that are located in the camera’s field of view with green lines in (b).

**Table S5:** Mean Inlier ratio, mean inlier amount and filter recall on KITTI dataset. For evaluating the filter’s performance, Add Corr. is not used.

	Mean Inlier Ratio(%)			Mean Inlier Amount			Filter Recall
	1.2m	0.6m	0.3m	1.2m	0.6m	0.3m	
LightGlue	55.9	42.8	28.0	72	55	37	-
FCGF	45.4	27.5	11.2	2054	1234	500	-
FCGF + LightGlue	93.6	64.0	25.4	1722	1192	485	97.3

experiments on ScanNet dataset. We notice that the valid LightGlue correspondences in KITTI dataset (the average is 129) are fewer than in ScanNet dataset (the average is 256) although the image size of KITTI ( $1226 \times 370$ ) is larger than ScanNet ( $640 \times 480$ ), which indicates that the visual correspondences in KITTI dataset are much sparser than in ScanNet dataset. Besides, the inlier ratio of visual correspondences in KITTI dataset is quite lower than in ScanNet dataset. These may be caused by the low image quality, large movement of camera or limited generalization of the pretrained model. Sparse and inaccuracy visual correspondences bring great challenge to the filter, however, our method can still remove a great amount of outliers via visual information, which demonstrates our method’s robustness. Furthermore, we evaluate the registration performance with different settings on KITTI dataset. We report rotation and translation accuracy under different thresholds and median error. Since the inlier ratio of LightGlue is considerably lower than in 3DMatch or ScanNet dataset, which deteriorates the registration performance of only LightGlue when

**Table S6:** Point cloud registration accuracy on KITTI dataset. By effectively combine the advantages of each feature, our method achieves a considerably better performance than using individual feature.

	Post Refi.	Rotation(deg)				Translation(m)			
		Accuracy $\uparrow$			Error $\downarrow$	Accuracy $\uparrow$			Error $\downarrow$
		2	5	10	Med.	0.5	1	2	Med.
FCGF		53.9	87.4	93.2	1.8	38.6	70.3	79.8	0.7
LightGlue		77.5	96.0	98.2	1.1	64.5	83.6	91.0	0.4
FCGF + LightGlue		91.5	97.8	98.7	0.7	91.0	94.8	95.3	0.2
FCGF + LightGlue	✓	96.4	98.0	98.6	0.5	93.2	95.5	96.2	0.1

using the Weighted Procrustes method. Therefore, we make comparisons with the RANSAC method for the geometric fitting rather than Weighted Procrustes. As shown in Tab. S6, significant performance improvement is achieved by our method compared to only FCGF or LightGlue, which demonstrates our method’s effectiveness and generalization.